




# Neutrino Counterparts of Fast Radio Bursts

Brian D. Metzger<sup>1</sup> , Ke Fang<sup>2,4</sup>, and Ben Margalit<sup>3,4</sup>

<sup>1</sup> Department of Physics, Columbia University, New York, NY 10027, USA; [bdm2129@columbia.edu](mailto:bdm2129@columbia.edu)

<sup>2</sup> Kavli Institute for Particle Astrophysics and Cosmology (KIPAC), Stanford University, Stanford, CA 94305, USA

<sup>3</sup> Astronomy Department and Theoretical Astrophysics Center, University of California, Berkeley, Berkeley, CA 94720, USA

Received 2020 August 27; revised 2020 September 21; accepted 2020 September 25; published 2020 October 12

## Abstract

The discovery of a luminous radio burst, FRB 200428, with properties similar to those of fast radio bursts (FRBs), in coincidence with an X-ray flare from the Galactic magnetar SGR 1935+2154, supports magnetar models for cosmological FRBs. The burst’s X-ray to radio fluence ratio, as well as the X-ray spectral shape and peak energy, are consistent with FRB 200428 being the result of an ultra-relativistic shock (powered, e.g., by an ejected plasmoid) propagating into a magnetized baryon-rich external medium; the shock simultaneously generates X-ray/gamma-rays via thermal synchrotron emission from electrons heated behind the shock, and coherent radio emission via the synchrotron maser mechanism. Here, we point out that a unique consequence of this baryon-loaded shock scenario is the generation of a coincident burst of high-energy neutrinos, generated by photohadronic interaction of relativistic ions—heated or accelerated at the shock—with thermal synchrotron photons. We estimate the properties of these neutrino burst FRB counterparts and find that a fraction  $\sim 10^{-8}$ – $10^{-5}$  of the flare energy (or  $\sim 10^{-4}$ – $10^{-1}$  of the radio isotropic energy) is channeled into production of neutrinos with typical energies  $\sim$ TeV–PeV. We conclude by discussing prospects for detecting this signal with IceCube and future high-energy neutrino detectors.

*Unified Astronomy Thesaurus concepts:* [Radio transient sources \(2008\)](#); [Cosmological neutrinos \(338\)](#); [Shocks \(2086\)](#); [Gamma-rays \(637\)](#); [Magnetars \(992\)](#)

## 1. Introduction

Fast radio bursts (FRBs) are millisecond-duration pulses of coherent radio emission of extragalactic origin (Lorimer et al. 2007; Thornton et al. 2013; see Cordes & Chatterjee 2019; Petroff et al. 2019 for reviews). Although many models have been proposed for FRBs (Platts et al. 2019), their central engines and emission mechanism remain elusive. The most well-studied class of models, which can for instance accommodate the discovery that many FRBs are observed to recur on timescales from minutes to weeks (e.g., Spitler et al. 2016; CHIME/FRB Collaboration et al. 2019), postulate an origin associated with flaring activity of magnetars (Popov & Postnov 2013; Kulkarni et al. 2014; Lyubarsky 2014; Katz 2016; Murase et al. 2016; Beloborodov 2017; Kumar et al. 2017; Metzger et al. 2017).

Magnetar FRB models received a recent jolt of support following the discovery of a double-peaked radio burst in spatial and temporal coincidence with a double-peaked hard X-ray outburst from the Galactic magnetar SGR 1935+2154 (Bochenek et al. 2020; The CHIME/FRB Collaboration et al. 2020). The energy radiated by the burst (hereafter FRB 200428) in the  $\sim$ GHz radio band,  $\mathcal{E}_{\text{radio}} \sim 10^{34}$ – $10^{35}$  erg, exceeds by several orders of magnitude that of any radio burst detected prior from a Galactic neutron star (including giant pulses from young pulsars like the Crab) and is within a factor of  $\lesssim 10$  of the least energetic cosmological FRBs of known distance.

The rate of bursts with similar energy and occurrence rate to FRB 200428 is itself insufficient to explain the total extragalactic FRB population, as inferred from the measured all-sky FRB rate. Nevertheless, if the same physical processes can be scaled-up to more energetic bursts, allowing for a more extreme

range of magnetar activity than seen in the Milky Way (as needed to explain particularly active recurrent sources like FRB 121102; Spitler et al. 2016), such a unified scenario can account for most or all of the cosmological FRB population (Lu et al. 2020b; Margalit et al. 2020b).

Despite the breakthrough discovery of FRB 200428, several open questions remain, particularly on the theory side. Chief among these is how to distinguish between several proposed variations of the magnetar model, which make qualitatively different predictions for the mechanism and location of the radio emission and the expectation (if any) of each for an accompanying higher-frequency afterglow. Unlike cosmological FRBs, for which no unambiguous multi-wavelength counterpart has yet been detected, the joint detection of X-ray and radio emission from FRB 200428 find a natural explanation in some magnetar models, while placing others in tension (Lu et al. 2020a; Margalit et al. 2020a).

Arguably the most well-developed of these models, in terms of making quantitative predictions for the burst properties motivated by first-principles kinetic plasma simulations, postulate that FRBs are the electromagnetic wave precursors of transient magnetized shocks generated by flare ejecta (e.g., an ultra-relativistically expanding plasmoid) released from the magnetosphere (Lyubarsky 2014; Beloborodov 2017). In these scenarios the radio precursor is generated at the shock front by electrons undergoing the synchrotron maser process (e.g., Gallant et al. 1992; Iwamoto et al. 2019; Plotnikov & Sironi 2019). The “synchrotron maser blast wave model” naturally accounts for the high observed linear polarization of many bursts (e.g., Ravi et al. 2016; Petroff et al. 2017), their complex spectral energy distribution (e.g., Babul & Sironi 2020), and the observed downward drifting of burst sub-pulses (e.g., CHIME/FRB Collaboration et al. 2019; Hessels et al. 2019) due to the decreasing Doppler factor as the blast wave

<sup>4</sup> NHFP Einstein Fellow.

**Table 1**  
Definitions

Symbol	Description
$E$	Proton energy
$\epsilon$	Photon energy
$\varepsilon$	Neutrino energy
$\mathcal{E}$	Total energy

decelerates as it sweeps up material (Metzger et al. 2019; Margalit et al. 2020b).

Even among magnetized shock models, there exist variations depending on the nature of the upstream medium into which the ultra-relativistic flare ejecta from the magnetar collides. Lyubarsky (2014) and Beloborodov (2017) postulated an upstream medium composed of electron/positron plasma, either representing a nebula surrounding the magnetar, or an ultra-relativistic spin-down powered wind, respectively. Metzger et al. (2019) instead considered the upstream medium to be a mildly relativistically expanding, baryon-loaded outflow with an electron-ion composition. Such an ambient environment may be generated by prior flaring activity. The existence of baryonic ejection is supported in at least the most powerful giant Galactic magnetar flares by radio afterglow emission indicating the presence of a trans-relativistic, mass-loaded outflow (Frail et al. 1999; Gelfand et al. 2005).

As shown by Margalit et al. (2020a) and recounted below, the predictions of the baryon-loaded electron-ion upstream model agree quantitatively with the properties of FRB 200428, provided that one interprets the hard X-ray emission from the flare (Mereghetti et al. 2020; Ridnaia et al. 2020; Tavani et al. 2020; Zhang et al. 2020) as incoherent synchrotron radiation from relativistically hot thermal electrons heated by the same shock generating the FRB. Because both the radio and X-ray emission originate from the same physical location, their nearly simultaneous observed arrival time—once accounting for the finite propagation speed of the radio burst through the Galactic interstellar medium (ISM)—is naturally expected (see also Yamasaki et al. 2020; Yuan et al. 2020). Margalit et al. (2020a) summarize several falsifiable predictions of this model, testable by future Galactic or nearby extragalactic FRBs (see also Beniamini & Kumar 2020; Lu et al. 2020a for criticisms of shock models).

An important consequence of an electron-ion upstream medium is the prediction at the shocks of heating, and potential nonthermal acceleration, of ions to relativistic energies. Unlike an electron/positron plasma, relativistic ions can generate neutrino emission via the photohadronic interaction with thermal synchrotron photons, similar to proposed mechanisms of neutrino emission in gamma-ray burst jets (Waxman & Bahcall 1997; Mészáros & Waxman 2001; Dermer & Atoyan 2003; Guetta & Granot 2003).

In this Letter, we estimate the properties of the neutrino bursts predicted to accompany FRBs in the synchrotron maser electron-ion blast wave scenario, and assess their detectability with the IceCube Neutrino Observatory. Tables 1 and 2 summarize several definitions that may be useful to refer to throughout the text.

## 2. Magnetized Relativistic Shocks

Following Metzger et al. (2019), we consider an ultra-relativistic blast wave generated by flare ejecta from the magnetar (e.g., a magnetically dominated plasmoid; e.g., Yuan et al. 2020) with an isotropic energy  $\mathcal{E}_{\text{flare}}$  propagating into an external electron-ion medium with a radial density profile  $n_{\text{ext}} \propto r^{-k}$ , where  $k < 3$  (we will soon specialize to the case  $k = 0$ ). We focus on observer times  $t$  greater than the intrinsic width of the flare ejecta  $\delta t$ , as is typically satisfied for FRBs of duration  $\gtrsim 1$  ms if the flare duration  $\delta t \sim \text{few} \times R_{\text{ns}}/c \sim 0.1$  ms is set by the Alfvén crossing time of the inner magnetosphere of a neutron star of radius  $R_{\text{ns}} \sim 10$  km.

The deceleration of the blast wave follows a self-similar evolution (Blandford & McKee 1976) resulting in the following evolution for the radius, Lorentz factor, and kinetic luminosity of the forward shock,

$$\Gamma = \Gamma_{\text{FRB}} \left( \frac{t}{t_{\text{FRB}}} \right)^{\frac{(k-3)}{2(4-k)}} \stackrel{k=0}{=} \Gamma_{\text{FRB}} \left( \frac{t}{t_{\text{FRB}}} \right)^{-\frac{3}{8}}, \quad (1)$$

$$r_{\text{sh}} = r_{\text{FRB}} \left( \frac{t}{t_{\text{FRB}}} \right)^{\frac{1}{(4-k)}} \stackrel{k=0}{=} r_{\text{FRB}} \left( \frac{t}{t_{\text{FRB}}} \right)^{\frac{1}{4}}, \quad (2)$$

$$n_{\text{ext}} = n_{\text{FRB}} \left( \frac{t}{t_{\text{FRB}}} \right)^{-\frac{k}{(4-k)}} \stackrel{k=0}{=} n_{\text{FRB}}, \quad (3)$$

$$L_{\text{sh}} = L_{\text{FRB}} \left( \frac{t}{t_{\text{FRB}}} \right)^{-1} \simeq \frac{\mathcal{E}_{\text{flare}}}{4t_{\text{FRB}}} \left( \frac{t}{t_{\text{FRB}}} \right)^{-1}, \quad (4)$$

where  $t_{\text{FRB}}$  is the observed duration of the FRB (as set by the timescale over which the spectral energy distribution of the maser emission sweeps downward across the observing band; Metzger et al. 2019) and  $\{\Gamma_{\text{FRB}}, r_{\text{FRB}}, n_{\text{FRB}}, L_{\text{FRB}}\}$  are the shock properties at  $t \sim t_{\text{FRB}}$ .

The latter quantities are related to observable properties of the FRB, namely its duration  $t_{\text{FRB}} = t_{\text{ms}}$  ms, radio frequency  $\nu_{\text{obs}} = \nu_{\text{GHz}}$  GHz, isotropic radio energy  $\mathcal{E}_{\text{radio}} = \mathcal{E}_{\text{r},40} 10^{40}$  erg, according to Margalit et al. (2020b)

$$r_{\text{FRB}} \approx 5 \times 10^{12} \text{cm} f_{\xi,-3}^{-2/15} \nu_{\text{GHz}}^{-7/15} t_{\text{ms}}^{1/5} \mathcal{E}_{\text{r},40}^{1/3}, \quad (5)$$

$$n_{\text{FRB}} \approx 420 \text{cm}^{-3} f_{\xi,-3}^{-4/15} \nu_{\text{GHz}}^{31/15} t_{\text{ms}}^{2/5} \mathcal{E}_{\text{r},40}^{-1/3}, \quad (6)$$

$$\Gamma_{\text{FRB}} \approx 287 f_{\xi,-3}^{-1/15} \nu_{\text{GHz}}^{-7/30} t_{\text{ms}}^{-2/5} \mathcal{E}_{\text{r},40}^{1/6} \quad (7)$$

where  $f_{\xi} = 10^{-3} f_{\xi,-3}$  is the efficiency of the maser emission, normalized to a characteristic value found by particle-in-cell (PIC) plasma simulations of magnetized shocks (Plotnikov & Sironi 2019; Babul & Sironi 2020) and we have assumed an upstream ratio of electrons to nucleons  $f_e = 0.5$  (the results can be easily generalized to include an electron–positron component).

The radiative efficiency of the FRB emission is given by Margalit et al. (2020b)

$$\eta \equiv \frac{\mathcal{E}_{\text{radio}}}{\mathcal{E}_{\text{flare}}} \approx 4 \times 10^{-5} f_{\xi,-3}^{4/5} \nu_{\text{GHz}}^{-1/5} t_{\text{ms}}^{-1/5}, \quad (8)$$

such that

$$\mathcal{E}_{\text{flare}} \approx 2.4 \times 10^{44} \text{erg} f_{\xi,-3}^{-4/5} \nu_{\text{GHz}}^{1/5} t_{\text{ms}}^{1/5} \mathcal{E}_{\text{r},40} \quad (9)$$

and the kinetic power of the shock at the epoch of FRB emission is given by

$$L_{\text{FRB}} \simeq \frac{\mathcal{E}_{\text{flare}}}{4t_{\text{FRB}}} \approx 6 \times 10^{46} \text{ erg s}^{-1} f_{\xi,-3}^{-4/5} \nu_{\text{GHz}}^{1/5} t_{\text{ms}}^{-4/5} \mathcal{E}_{r,40} \quad (10)$$

The population of cosmological FRBs with known distances exhibit typical ranges  $\mathcal{E}_{\text{radio}} \sim 10^{37}\text{--}10^{41}$  erg,  $t_{\text{FRB}} \sim 0.1\text{--}10$  ms, such that one infers  $r_{\text{FRB}} \sim 10^{12}\text{--}10^{13}$  cm,  $\Gamma_{\text{FRB}} \sim 10^2\text{--}10^3$ , and  $n_{\text{FRB}} \sim 10^2\text{--}10^4$  cm $^{-3}$  (Margalit et al. 2020b). From the observed rate of downward frequency drifting of the sub-pulses, which in this model could arise from deceleration of the blast wave (Metzger et al. 2019), one infers power-law indices of the external medium spanning a wide-range  $k \approx [-2, 2]$  (Margalit et al. 2020b). In what follows we assume a constant density medium ( $k=0$ ) for simplicity, though this too can be easily generalized and our results to follow do not depend qualitatively on this assumption.

From Equations (4) and (7), the blast wave transitions from ultra-relativistic to non-relativistic expansion ( $\Gamma \simeq 1$ ) after a time

$$t_{\text{nr}} \simeq t_{\text{FRB}} \Gamma_{\text{FRB}}^{8/3} \simeq 3.5 \times 10^3 \text{ s } f_{\xi,-3}^{-8/45} \nu_{\text{GHz}}^{-28/45} t_{\text{ms}}^{-1/15} \mathcal{E}_{r,40}^{4/9}, \quad (11)$$

which is minutes to hours for typical parameters.

In addition to generating the coherent FRB emission, the shock heats the plasma to ultra-relativistic temperatures. Again guided by the results of PIC simulations of magnetized shocks, we assume that the post-shock energy is shared roughly equally with the electrons and ions, heating each to a Maxwellian distribution of energies (e.g., Sironi & Spitkovsky 2011). Given the strong magnetic field behind the shock, the electrons radiate (incoherent) synchrotron emission. The latter peaks at a photon energy (Metzger et al. 2019)

$$\epsilon_{\text{pk}} = \frac{\hbar e B'}{m_e c} \bar{\gamma}^2 \Gamma, \quad (12)$$

where  $\bar{\gamma} = (m_p/m_e)\Gamma/2$  is the mean thermal Lorentz factor,  $B' = \sqrt{64\pi\sigma\Gamma^2 m_p c^2 n_{\text{ext}}}$  is the post-shock magnetic field, and  $\sigma$  is the magnetization of the upstream medium. Thus we have

$$\epsilon_{\text{pk}} \approx 235 \text{ MeV } \sigma_{-1}^{1/2} f_{\xi,-3}^{-2/5} \nu_{\text{GHz}}^{1/10} \mathcal{E}_{r,40}^{1/2} t_{\text{ms}}^{-7/5} \left( \frac{t}{t_{\text{FRB}}} \right)^{-3/2}, \quad (13)$$

in the hard X-ray/ $\gamma$ -ray range, where  $\sigma_{-1} \equiv \sigma/(0.1)$ .<sup>5</sup> The cooling frequency is given by

$$\begin{aligned} \epsilon_c &= \frac{\hbar e B'}{m_e c} \gamma_c^2 \Gamma \\ &\approx 0.023 \text{ MeV } \sigma_{-1}^{-3/2} f_{\xi,-3}^{2/3} \nu_{\text{GHz}}^{-65/30} t_{\text{ms}}^{-1} \mathcal{E}_{r,40}^{-1/6} \left( \frac{t}{t_{\text{FRB}}} \right)^{-1/2}, \quad (14) \end{aligned}$$

<sup>5</sup> The value of  $\sigma$  in the baryon-loaded upstream is uncertain. A minimum value  $\sigma \gtrsim 10^{-3}$  is required for operation of the synchrotron maser, while very large values  $\sigma \gg 1$  are also disfavored due to the declining radiative efficiency with increasing  $\sigma$  (Plotnikov & Sironi 2019).

where  $\gamma_c = (6\pi m_e c / \sigma_T \Gamma B'^2 t)$  is the Lorentz factor of the electrons that cool on the expansion time. The post-shock electrons thus remain fast-cooling ( $\epsilon_c \lesssim \epsilon_{\text{pk}}$ ) for a timescale

$$t_c \approx 10 \text{ s } \sigma_{-1}^2 f_{\xi,-3}^{-16/15} \nu_{\text{GHz}}^{34/15} t_{\text{ms}}^{3/5} \mathcal{E}_{r,40}^{2/3}, \quad (15)$$

much longer than the FRB duration; thus the radiated X-ray/ $\gamma$ -ray energy  $E_{X/\gamma} \approx \mathcal{E}_{\text{flare}}/2$  is equal to that given to the electrons.

Considering the application to FRB 200428 (Margalit et al. 2020b), the value  $\eta \sim 10^{-4}\text{--}10^{-5}$  predicted by Equation (8) agrees with the measured ratio of the radio and X-ray fluence ( $\mathcal{E}_{\text{radio}} \sim 10^{34}\text{--}10^{35}$  erg; Bochenek et al. 2020; The CHIME/FRB Collaboration et al. 2020;  $E_{X/\gamma} \sim 10^{39}\text{--}10^{40}$  erg; Mereghetti et al. 2020; Zhang et al. 2020) for  $f_{\xi} \sim 10^{-3}$ . For the same parameters (e.g.  $\mathcal{E}_{r,40} \sim 10^{-5}$ ), Equation (13) predicts a peak frequency (given the observed duration  $t \sim 3$  ms of the X-ray spikes of FRB 200428) of  $\epsilon_{\text{pk}} \sim 300 \sigma_{-1}^{1/2}$  keV, which is also consistent with the spectral peak of the observed power-law X-ray/ $\gamma$ -ray emission. Finally, the energy spectrum of the X-ray/ $\gamma$ -ray emission is well fit by a power law + cut-off (e.g., Mereghetti et al. 2020), which is similar to predictions for a fast-cooling thermal synchrotron spectrum (Giannios & Spitkovsky 2009). Taken together, these observations support a magnetized shock propagating into a baryon-loaded medium as the origin of FRB 200428 and its associated X-ray burst (Margalit et al. 2020a).

### 3. High-energy Neutrino Emission

#### 3.1. Proton Heating and Acceleration

A fraction  $\sim 1/2$  of the shock's energy goes into thermally heating ions, which hereafter we take to be protons for simplicity. The protons achieve a relativistic Maxwellian distribution with an average particle energy of  $\bar{E}' \approx \Gamma m_p c^2/2$  in the co-moving frame of the shocked gas (hereafter denoted by a prime'). Though less certain, particularly for a strongly magnetized upstream ( $\sigma \gg 1$ ), the shocks may accelerate a small fraction of the protons to higher energies  $\gg \bar{E}'$  (e.g., via diffusive acceleration; Blandford & Ostriker 1978), into a power-law nonthermal spectrum of the form

$$\frac{dN'_p}{dE'} \propto \left( \frac{E'}{\bar{E}'} \right)^{-q}, \quad \bar{E}' < E' < E'_{\text{max}}, \quad (16)$$

where  $E'_{\text{max}}$  is a maximum cut-off energy, to be estimated below. Taking  $q \simeq 2$ , the fraction of the total shock kinetic luminosity placed into protons of energy  $\sim E' \geq \bar{E}'$  can be roughly written as

$$f_{E'} \approx \begin{cases} 1/2 & E' \sim \bar{E}' \\ \epsilon_{\text{rel}}/\Lambda & E' \gg \bar{E}', \end{cases} \quad (17)$$

where  $\epsilon_{\text{rel}} \lesssim 0.1$  is an acceleration efficiency and  $\Lambda \equiv \ln(E'_{\text{max}}/\bar{E}') \sim 10$  (see below).

In order to estimate the value of  $E'_{\text{max}}$  we equate the proton acceleration time (estimated by the Larmor gyration time)  $t_{\text{acc}} \sim 2\pi E'/eB'c$  to various loss timescales. The most stringent constraint<sup>6</sup> comes from equating  $t_{\text{acc}}$  to the dynamical time,

<sup>6</sup> Other proton-loss timescales, such as due to synchrotron cooling, are much longer—and hence unconstraining on  $E_{\text{max}}$ —than the dynamical timescale for shock parameters of interest.

**Table 2**  
Key Timescales and Energies

Symbol	Description	Typical Values <sup>a</sup>
$t_{\text{FRB}}$	FRB duration	$\sim 0.1\text{--}10$ ms
$t_{\text{nth}}$ (Equation (22))	Duration of $\nu$ 's from thermal protons	$\sim 0.1 - 1$ ms
$t_c$ (Equation (15))	Synchrotron emission no longer fast-cooling	$\sim 0.1\text{--}10^3$ s
$t_{\text{max}}$ (Equation (25))	Duration of $\nu$ 's from nonthermal protons	$\sim 1\text{--}10^3$ s
$t_{\text{nr}}$ (Equation (11))	Transition to non-relativistic shock	$\sim 10^2\text{--}10^5$ s
$\bar{E}$	Mean thermal energy of protons	$\sim 10\text{--}100$ GeV <sup>b</sup>
$\epsilon_{\text{pk}}$ (Equation (13))	Synchrotron peak photon energy	$\sim 10\text{--}10^3$ eV
$\epsilon_c$ (Equation (14))	Synchrotron cooling photon energy	$\sim 10\text{--}10^3$ eV
$\epsilon_c$ (Equation (27))	Peak energy of neutrino spectrum ( $t < t_c$ )	$\sim 0.1\text{--}10$ PeV
$\epsilon_{\text{min}}$ (Equation (23))	Minimum energy of neutrino spectrum	$\sim 1\text{--}10$ PeV
$\epsilon_{\text{max}}$ (Equation (24))	Maximum energy of neutrino spectrum	$\sim 1\text{--}10$ PeV

**Notes.**

<sup>a</sup> For  $\sigma \sim 0.1$  and  $\mathcal{E}_{\text{rad}} \sim 10^{37}\text{--}10^{43}$  erg in the range of cosmological FRB.

<sup>b</sup> For energies we quote values on the timescale  $\sim t_{\text{max}}$ .

$t_{\text{dyn}} \simeq r_{\text{sh}}/(\Gamma c)$ , over which adiabatic losses occur. This gives

$$E'_{\text{max}} \simeq \frac{eB'r_{\text{sh}}}{2\pi\Gamma} = e r_{\text{sh}} c \sqrt{(16/\pi)\sigma m_p n_{\text{ext}}} \\ \approx 850 \text{ TeV} \sigma_{-1}^{1/2} f_{\xi,-3}^{-4/15} \nu_{\text{GHz}}^{17/30} t_{\text{ms}}^{2/5} \mathcal{E}_{r,40}^{1/6} \left(\frac{t}{t_{\text{FRB}}}\right)^{1/4}. \quad (18)$$

Note that  $E'_{\text{max}} \sim 1 \text{ PeV} \sim 10^3\text{--}10^4 \bar{E}'$  on the timescale of the FRB  $t \sim t_{\text{FRB}}$ , increasing by  $t \sim t_{\text{nr}}$  to  $\gtrsim 10 \text{ PeV}$ .

### 3.2. Pion Production and Neutrino Emission

Although the electrons generally cool faster than the dynamical timescale at early times ( $t \ll t_c$ ; Equation (15)), this is not true of the protons due to their greater mass. The protons retain their energy, enabling them to interact with the thermal synchrotron photons via the photomeson process  $p + \gamma \rightarrow p + \pi^{\pm,0}$  (Berezinskii et al. 1990), generating high-energy gamma-rays and neutrinos via the decay of  $\pi^0$  and  $\pi^{\pm}$ , respectively. The rate of hadronuclear interactions (e.g.  $p + p \rightarrow p + p + \pi^{\pm,0}$ ) are low in comparison because of the high photon-to-baryon ratio behind the shock.

The energy distribution of the thermal synchrotron emission from the electrons peaks at a photon energy

$$\epsilon'_{\text{pk}} \approx \frac{\epsilon_{\text{pk}}}{\Gamma} \approx 0.8 \text{ MeV} \sigma_{-1}^{1/2} f_{\xi,-3}^{-1/3} \nu_{\text{GHz}}^{1/3} t_{\text{ms}}^{-1} \mathcal{E}_{r,40}^{1/3} \left(\frac{t}{t_{\text{FRB}}}\right)^{-9/8}, \quad (19)$$

where we have used Equations (7) and (13). Immersed in this radiation field, pion production peaks at the  $\Delta$ -resonance at a proton energy (e.g., Waxman & Bahcall 1997)

$$E'_{\text{thr}} \approx \frac{E'_{\Delta} m_p c^2}{\epsilon'_{\text{pk}} 2} \\ \approx 170 \text{ GeV} \sigma_{-1}^{-1/2} f_{\xi,-3}^{1/3} \nu_{\text{GHz}}^{-1/3} t_{\text{ms}} \mathcal{E}_{r,40}^{-1/3} \left(\frac{t}{t_{\text{FRB}}}\right)^{9/8}, \quad (20)$$

where  $E'_{\Delta} \approx 0.3 \text{ GeV}$ . Comparing this threshold to the proton thermal energy,

$$\frac{E'_{\text{thr}}}{\bar{E}'} \approx \frac{2E'_{\text{thr}}}{\Gamma m_p c^2} \approx \frac{E'_{\Delta}}{\epsilon_{\text{pk}}} \\ \approx 1.3 \sigma_{-1}^{-1/2} f_{\xi,-3}^{2/5} \nu_{\text{GHz}}^{-1/10} t_{\text{ms}}^{7/5} \mathcal{E}_{r,40}^{-1/2} \left(\frac{t}{t_{\text{FRB}}}\right)^{3/2}. \quad (21)$$

Thus, on timescales of the FRB emission ( $t \sim t_{\text{FRB}}$ ), protons which are either thermal ( $E' \sim \bar{E}'$ ), or only moderately into the nonthermal tail ( $E' \gtrsim \bar{E}'$ ; Equation (16)), are capable of pion-producing on synchrotron photons. However, at times  $t \gg t_{\text{FRB}}$ , only the nonthermal protons with  $E' \gg \bar{E}'$  have enough energy to produce pions. This transition ( $\bar{E}' = E'_{\text{thr}}$ ) from thermal to nonthermal-only production occurs at a time

$$t_{\text{nth}} \approx 8.5 \times 10^{-4} \text{ s} \sigma_{-1}^{1/3} f_{\xi,-3}^{-4/15} \nu_{\text{GHz}}^{1/15} t_{\text{ms}}^{1/15} \mathcal{E}_{r,40}^{1/3}. \quad (22)$$

The pions generated decay into neutrinos of lab-frame energy  $\epsilon \approx \Gamma E'/20$  (Kelner & Aharonian 2008). The minimum neutrino energy at time  $t$  is therefore

$$\epsilon_{\text{min}} \approx \max[\Gamma \bar{E}'/20, \Gamma E'_{\text{thr}}/20] \\ \approx \max \begin{cases} 1.9 \text{ TeV} f_{\xi,-3}^{-2/15} \nu_{\text{GHz}}^{-7/15} t_{\text{ms}}^{-4/5} \mathcal{E}_{r,40}^{1/3} \left(\frac{t}{t_{\text{FRB}}}\right)^{-3/4}, & t \lesssim t_{\text{nth}} \\ 2.5 \text{ TeV} \sigma_{-1}^{-1/2} f_{\xi,-3}^{4/15} \nu_{\text{GHz}}^{-17/30} t_{\text{ms}}^{3/5} \mathcal{E}_{r,40}^{-1/6} \left(\frac{t}{t_{\text{FRB}}}\right)^{3/4}, & t \gtrsim t_{\text{nth}} \end{cases} \quad (23)$$

From Equation (18), one can also define an absolute maximum neutrino energy, as set by the accelerator,

$$\epsilon_{\text{max}} \approx \frac{\Gamma E'_{\text{max}}}{20} \approx 12 \text{ PeV} \sigma_{-1}^{1/2} f_{\xi,-3}^{-1/3} \nu_{\text{GHz}}^{1/3} \mathcal{E}_{r,40}^{1/3} \left(\frac{t}{t_{\text{FRB}}}\right)^{-1/8} \quad (24)$$

Equating  $\epsilon_{\text{min}}(t > t_{\text{nth}})$  (Equation (23)) to  $\epsilon_{\text{max}}$ , we obtain

$$t_{\text{max}} \approx 17 \text{ s} \sigma_{-1}^{8/7} f_{\xi,-3}^{-24/35} \nu_{\text{GHz}}^{36/35} t_{\text{ms}}^{11/35} \mathcal{E}_{r,40}^{4/7}. \quad (25)$$

This is the maximal timescale for significant neutrino emissions because at  $t > t_{\text{max}}$  the proton energy required to interact with

the most energetic synchrotron photons (of energy  $\sim \epsilon_{\text{pk}}$ ) exceeds  $E_{\text{max}}$ .

Before  $t_{\text{max}}$ , higher-energy neutrinos with  $\epsilon_{\text{min}} < \epsilon < \epsilon_{\text{max}}$  can be created by the interaction of protons with energies  $E' \gg E'_{\text{thr}}$ ,  $\bar{E}'$  with photons of lower energies  $\epsilon' \ll \epsilon'_{\text{pk}}$  below the synchrotron peak. In fact, while the synchrotron emission is fast-cooling ( $t < t_c$ ; Equation (15)) such interactions dominate neutrino production (by nonthermal protons) because the photon number spectrum in the fast-cooling regime,

$$\epsilon (dN_\gamma/d\epsilon) \propto \epsilon^{-1/2}, \quad \epsilon_c \lesssim \epsilon \lesssim \epsilon_{\text{pk}}, \quad (26)$$

peaks at  $\epsilon_c < \epsilon_{\text{pk}}$ .<sup>7</sup>

In the fast-cooling regime the energy distribution of neutrinos from nonthermal protons will thus peak at an energy,

$$\begin{aligned} \epsilon_c &\approx \frac{\Gamma E'_\Delta m_p c^2}{20 \epsilon'_c} \\ &\approx 26 \text{ PeV } \sigma_{-1}^{3/2} f_{\xi,-3}^{-4/5} \nu_{\text{GHz}}^{17/10} t_{\text{ms}}^{1/5} \mathcal{E}_{r,40}^{1/2} \left( \frac{t}{t_{\text{FRB}}} \right)^{-1/4}, \end{aligned} \quad (27)$$

where  $\epsilon'_c = \epsilon_c/\Gamma$ . The value of  $\epsilon_c$  decreases in time, matching  $\epsilon_{\text{min}}$  at  $t = t_c$ .

In principle, pions and muons could suffer synchrotron losses before decaying into neutrinos. This happens above a energy critical energy

$$\begin{aligned} \epsilon_{\pi,\mu}^{\text{syn}} &= \left( \frac{6\pi m_{\pi,\mu} c}{\sigma_T B'^2 \tau_{\pi,\mu}} \right)^{1/2} \left( \frac{m_{\pi,\mu}}{m_e} \right) m_{\pi,\mu} c^2 \Gamma \\ &= (30, 1.7) \times 10^{18} \text{ eV } \sigma_{-1}^{-1/2} f_{\xi,-3}^{2/15} \nu_{\text{GHz}}^{-31/30} t_{\text{ms}}^{-1/5} \mathcal{E}_{r,40}^{1/6}, \end{aligned} \quad (28)$$

where  $m_\pi$ ,  $\mu$  and  $\tau_\pi$ ,  $\mu$  are the masses and rest-frame lifetimes of pions and muons, respectively. Because  $\epsilon_\pi^{\text{syn}} \gg 4 \epsilon_{\text{max}}$  and  $\epsilon_\mu^{\text{syn}} \gg 3 \epsilon_{\text{max}}$  (where the prefactors account for the rough energy partition between pions/muons/neutrinos in the decays), we conclude that synchrotron cooling of the secondaries is negligible.

In summary, although all of the timescales increase with the flare energy, the hierarchy  $t_{\text{nth}} < t_c < t_{\text{max}} < t_{\text{nr}}$  is generally preserved for  $\sigma \lesssim 1$  and moderate variations around fiducial parameters (Table 2). At early times ( $t \lesssim t_{\text{nth}}$ ) we expect  $\sim 1$ – $10$  TeV neutrinos generated by the interaction of the thermal protons with synchrotron photons of energy  $\sim \epsilon_{\text{pk}}$ . This prediction is relatively robust (within the baryon shock model) because proton heating at the shocks is inevitable. Furthermore, because  $t_{\text{nth}} \sim t_{\text{FRB}}$  the thermal neutrino emission occurs simultaneously with the FRB emission, and hence we do not need to assume a continuation of the external medium outside the region directly probed by radio observations.

At later times ( $t \gtrsim t_{\text{nth}}$ ) the thermal protons are soon no longer sufficiently energetic to produce pions, but nevertheless neutrinos may still be produced by the power-law nonthermal protons. Insofar as the proton spectrum is flat ( $q \simeq 2$ ), the dominant interaction while the synchrotron emission is fast-cooling ( $t \ll t_c$ ) will be between photons of energy  $\sim \epsilon_c \ll \epsilon_{\text{pk}}$  on high-energy protons  $\sim 20 \epsilon_c$  generating neutrinos of energy  $\epsilon_c \sim 1$ – $10$  PeV. However, at times  $t \gg t_c$  the synchrotron spectrum becomes slow-cooling and the

interaction will be dominated by photons of energy  $\sim \epsilon_{\text{pk}}$  generating neutrinos of energy  $\epsilon_{\text{min}}(t \gtrsim t_c) \gtrsim 10$  PeV.

### 3.3. Neutrino Radiative Efficiency

What fraction of the available proton luminosity  $\sim L_{\text{sh}}/2$  will be radiated as neutrinos? One can define an ‘‘optical depth’’ for neutrino production over each decade in observer time  $\sim t$ ,

$$\tau_{p\gamma} \approx n'_\gamma \sigma_{p\gamma} \kappa_{p\gamma} r' \quad (29)$$

where  $n'_\gamma$  is the target photon number density given below,  $r' \approx r_{\text{sh}}/\Gamma$  is the characteristic radius of the post-shock region in the co-moving frame (through which relativistic protons accelerated at the shock traverse to escape without losses),  $\sigma_{p\gamma}$  is the cross section of photopion production, which is  $\sim 5 \times 10^{-28} \text{ cm}^2$  (Particle Data Group et al. 2004) corresponding to its value near the  $\Delta$ -resonance (and  $\sim 1.6 \times 10^{-28} \text{ cm}^2$  above the resonance). The factor  $\kappa_{p\gamma} \sim 0.15$  is the average fraction of energy lost from a proton per collision (‘‘elasticity’’). Consider first proton interactions with photons of energy  $\epsilon = \epsilon_{\text{pk}}$  that generate neutrinos of energy  $\epsilon_{\text{min}}$  (Equation (23)). Their number density is given by  $n'_\gamma \approx U'_\gamma/\epsilon'_{\text{pk}}$ , where

$$U'_\gamma \approx \frac{L_{\text{sh}}/2}{4\pi r_{\text{sh}}^2 c \Gamma^2} \begin{cases} 1 & t \leq t_c \\ (t/t_c)^{-1/2} & t \geq t_c, \end{cases} \quad (30)$$

where the factor of  $1/2$  in the numerator arises from the half of the shock power placed into electrons in the fast-cooling regime. The factor  $(t/t_c)^{-1/2}$  factor accounts for the reduction in the radiated power when the electrons become slow-cooling at  $t \gtrsim t_c$  (Equation (15)).

Combining with the above

$$\begin{aligned} \tau_{p\gamma}[\epsilon_{\nu,\text{min}}] &\approx \frac{L_{\text{sh}} \sigma_{p\gamma} \kappa_{p\gamma}}{8\pi r_{\text{sh}} c \Gamma^2 \epsilon_{\text{pk}}} \begin{cases} 1 & t \leq t_c \\ (t/t_c)^{-1/2} & t \geq t_c, \end{cases} \\ &\approx 3.9 \times 10^{-8} \sigma_{-1}^{-1/2} f_{\xi,-3}^{-2/15} \nu_{\text{GHz}}^{31/30} t_{\text{ms}}^{6/5} \mathcal{E}_{r,40}^{-1/6} \\ &\times \begin{cases} \left( \frac{t}{t_{\text{FRB}}} \right) & t \leq t_c \\ \left( \frac{t_c}{t_{\text{FRB}}} \right) \left( \frac{t}{t_c} \right)^{1/2} & t \geq t_c \end{cases} \end{aligned} \quad (31)$$

At time  $t \lesssim t_c$ , the photon density  $n_\gamma$  at  $\epsilon = \epsilon_c$  is larger by a factor  $(t/t_c)^{-1/2}$  than at  $\epsilon_{\text{pk}}$  (Equation (26)); thus, the optical depth to generating  $\epsilon_{\nu,c}$  neutrinos is larger by the same factor:

$$\begin{aligned} \tau_{p\gamma}[\epsilon_{\nu,c}] &\approx \tau_{p\gamma}[\epsilon_{\nu,\text{min}}] (t/t_c)^{-1/2} \\ &\approx 3.9 \times 10^{-6} \sigma_{-1}^{1/2} f_{\xi,-3}^{-2/3} \nu_{\text{GHz}}^{65/30} t_{\text{ms}} \mathcal{E}_{r,40}^{1/6} \left( \frac{t}{t_{\text{FRB}}} \right)^{1/2}, \quad t \leq t_c \end{aligned} \quad (32)$$

Interestingly,  $\tau_{p,\gamma}$  at the peak of the neutrino energy spectrum increases  $\propto t^{1/2}$  in both fast- and slow-cooling regimes (both before and after  $t_c$ ). The fluence emitted in neutrinos over a

<sup>7</sup> When the shock is no longer fast cooling at times  $t \gtrsim t_c$  the spectrum below  $\epsilon_{\text{pk}}$  steepens to the standard slow-cooling spectrum  $\epsilon (dN_\gamma/d\epsilon) \propto \epsilon^{1/3}$  for which photons of energy  $\epsilon_{\text{pk}}$  dominate by both energy and number.

timescale  $\sim t$  is thus given by

$$\begin{aligned} \mathcal{E}_\nu &\approx \frac{3}{8} \int \tau_{p\gamma} f_{E'} L_{\text{sh}} dt \sim \frac{3}{8} \tau_{p\gamma} f_{E'} L_{\text{sh}} t \\ &\approx 8.9 \times 10^{37} \text{erg} f_{E'} \sigma_{-1}^{1/2} f_{\xi,-3}^{-22/15} \nu_{\text{GHz}}^{71/30} t_{\text{ms}}^{6/5} \mathcal{E}_{r,40}^{7/6} \left( \frac{t}{t_{\text{FRB}}} \right)^{1/2} \end{aligned} \quad (33)$$

where the factor  $3/8$  accounts for the fraction of the proton energy that goes into neutrino products (Waxman & Bahcall 1999) and  $f_{E'} \sim 0.01 - 0.5$  (Equation (17)) is the fraction of the shock power placed into protons obeying the threshold condition.

One can define a dimensionless neutrino radiative efficiency,

$$\begin{aligned} \eta_\nu &\equiv \frac{\mathcal{E}_\nu}{\mathcal{E}_{\text{flare}}} \approx \frac{3}{32} \tau_{p\gamma} [\varepsilon_{\nu,c}] f_{E'} \\ &\approx 3.7 \times 10^{-7} f_{E'} \sigma_{-1}^{1/2} f_{\xi,-3}^{-2/3} \nu_{\text{GHz}}^{65/30} t_{\text{ms}} \mathcal{E}_{r,40}^{1/6} \left( \frac{t}{t_{\text{FRB}}} \right)^{1/2} \end{aligned} \quad (34)$$

which is valid at all times  $t_{\text{FRB}} \lesssim t \lesssim t_{\text{max}}$ .

During the early epoch  $t \lesssim t_{\text{nth}}$ , when neutrinos are produced by thermal protons, we have  $f_{E'} \sim 0.5$  (Equation (17)) and hence  $\eta_\nu \sim 10^{-7} - 10^{-6}$  for fiducial parameters. At times  $t \gg t_{\text{nth}} \sim t_{\text{FRB}}$  when only nonthermal protons can produce neutrinos, we have  $f_{E'} \sim 10^{-2}$  if the shocks place a fraction  $\varepsilon_{\text{rel}} \sim 0.1$  of their energy into the power-law tail. Although the efficiency starts low in this case, it grows in time  $\eta_\nu \propto t^{1/2}$  until reaching a peak value once  $t \sim t_{\text{max}}$  of

$$\begin{aligned} \eta_\nu[t_{\text{max}}] &\approx 4.8 \times 10^{-7} \left( \frac{f_{E'}}{10^{-2}} \right) \\ &\times \sigma_{-1}^{15/14} f_{\xi,-3}^{-106/105} \nu_{\text{GHz}}^{563/210} t_{\text{ms}}^{23/35} \mathcal{E}_{r,40}^{19/42}, \end{aligned} \quad (35)$$

corresponding to a total radiated neutrino energy

$$\begin{aligned} \mathcal{E}_\nu &= \eta_\nu[t_{\text{max}}] \mathcal{E}_{\text{flare}} \\ &\approx 1.1 \times 10^{38} \text{erg} \left( \frac{f_{E'}}{10^{-2}} \right) \sigma_{-1}^{15/14} f_{\xi,-3}^{-38/21} \nu_{\text{GHz}}^{121/42} t_{\text{ms}}^{6/7} \mathcal{E}_{r,40}^{61/42}. \end{aligned} \quad (36)$$

The total neutrino emission from the shocks peaks at an energy,

$$\varepsilon_{\text{max}}[t_{\text{max}}] \approx 3.6 \text{ PeV} \sigma_{-1}^{5/14} f_{\xi,-3}^{-26/105} \nu_{\text{GHz}}^{43/210} \mathcal{E}_{r,40}^{11/42} t_{\text{ms}}^{3/35} \quad (37)$$

which scales weakly with FRB properties and model parameters.

Figure 1 shows an example calculation of the characteristic energies versus time, while Figure 2 shows the build-up of the neutrino spectrum with time as the shock propagates outwards (bottom panel). Figure 3 shows several key properties related to neutrino emission—such as the duration, spectral peak, total radiated energy, and fluence—for a sample of FRBs with measured properties ( $t_{\text{FRB}}$ ,  $\mathcal{E}_{\text{radio}}$ ,  $\nu_{\text{obs}}$ ) and known distances. Approximate IceCube sensitivity curves<sup>8</sup> are shown for comparison.

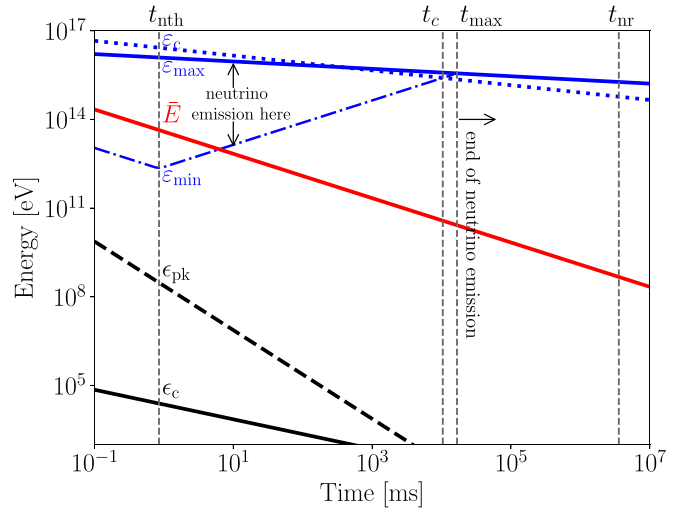


**Figure 1.** Critical energies as a function of time for a fiducial model with FRB duration  $t_{\text{FRB}} = 1$  ms, shock magnetization  $\sigma = 0.1$ , radiative efficiency of shock radio emission  $f_\xi = 10^{-3}$ , radio observing frequency  $\nu = 1$  GHz, and FRB isotropic energy  $\mathcal{E}_{\text{radio}} = 10^{40}$  erg.

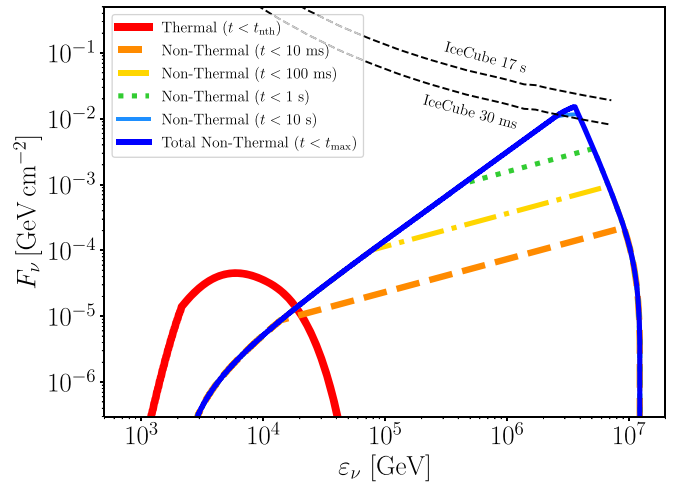


**Figure 2.** Observed muon neutrino spectra for the same model in Figure 1, showing the growth of the spectra over decades in time as the shock propagates outwards. Shown for comparison are approximate IceCube sensitivity curves for observation windows of 30 ms and 17 s, corresponding roughly to the duration of neutrino emission from thermal and nonthermal protons, respectively, for a source distance of 0.1 kpc.

#### 4. Detection Prospects

The upshot of our work is the prediction of an efficiency of up to  $\eta_\nu \sim 10^{-8} - 10^{-5}$  (Equation (35); Figure 3) for converting magnetar flare energy into a neutrino burst of energy  $\sim 1 - 10$  PeV, near the peak sensitivity range of IceCube. The energy radiated in neutrinos is typically  $\sim 10 - 100$  times smaller than the radio isotropic energy, making the signal extremely challenging to detect.

Consider first the recent FRB 200428 from the Galactic magnetar SGR 1935+2154. Taking  $\mathcal{E}_{\text{flare}} \sim 2E_{X/\gamma} \sim 10^{40}$  erg, we predict a neutrino burst of energy  $\mathcal{E}_\nu \lesssim 10^{32}$  erg, corresponding to a fluence (given an assumed source distance of 10 kpc) of  $F_\nu \sim 10^{-12}$  GeV cm<sup>-2</sup> (Figure 3). This is  $\sim 11$  orders of magnitude smaller than the IceCube upper limit of  $5 \times 10^{-2}$  GeV cm<sup>-2</sup> (Vandenbroucke 2020). Thus, the

<sup>8</sup> These are obtained by scaling the max-burst sensitivity of Aartsen et al. (2020) for a power-law spectrum  $E^{-2}$  with the detector effective area to northern-sky events.

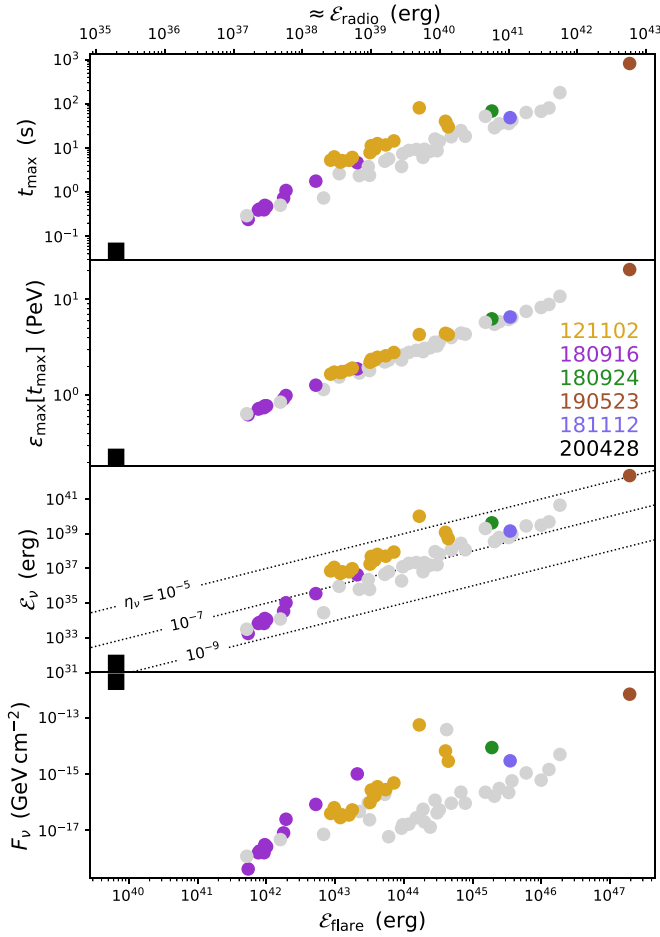


**Figure 3.** Predicted neutrino properties for a sample of FRBs with measured properties and known distances, as a function of the total flare energy (bottom axis) or approximate radio isotropic energy (top axis, assuming for simplicity a fixed radio efficiency  $\eta = 3 \times 10^{-5}$ ). Properties shown include the total radiated energy in neutrinos  $\mathcal{E}_\nu$  (Equation (36)), duration of neutrino emission  $t_{\max}$  (Equation (25)), peak neutrino energy  $\epsilon_{\max}(t_{\max})$  (Equation (37)), and neutrino flux  $F_\nu$ . The FRBs shown include the sample of localized FRBs with known distances (different colors, as labeled) and non-localized CHIME FRBs (gray points), as in Margalit et al. (2020a, 2020b).

neutrino non-detection of FRB 200428 is not constraining on the baryon shock model.

What about a more energetic Galactic magnetar flare? Although no FRB was detected in association with the 2004 giant flare from SGR 1806-20 (Tendulkar et al. 2016), this could be explained if the shock-generated plasmoid ejection was directed away from our line of sight (in which case the FRB would be dimmer due to relativistic beaming effects). Assuming a more fortuitous geometry of a future flare and scaling  $\mathcal{E}_{\text{flare}}$  up by a factor of  $\sim 10^6$  to the  $\sim 10^{46}$  erg energy scale of the gamma-ray emission from giant flares, the predicted flux for the nearest magnetar (1E 1048.1–5937 at  $\approx 2.7$  kpc; Gaensler et al. 2005) could reach  $\sim 10^{-2}$  GeV cm $^{-2}$ . In this case the detection of a neutrino from a giant flare becomes potentially feasible (see also Gelfand et al. 2005), particularly given proposed future upgrades to neutrino detectors (e.g., The IceCube-Gen2 Collaboration et al. 2020). Note that an FRB energy  $\gtrsim 10^{12}$  Jy ms is thus required to produce detectable neutrino emission in this case.

Individual extragalactic FRBs discovered to date are unlikely to be detectable due to their much greater distances (bottom

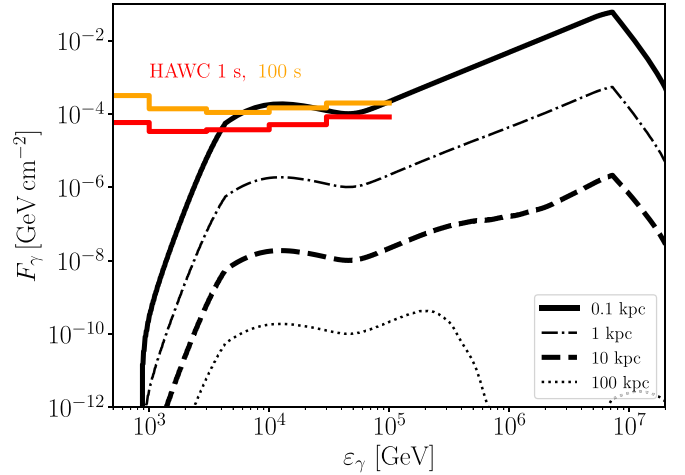


**Figure 4.** Total  $\gamma$ -ray fluence due to neutral pion decay from a fiducial burst as the one shown in Figure 2 at a distance of 0.1, 1, 10 and 100 kpc, comparing to the sensitivities of the HAWC Observatory at  $0^\circ$  zenith angle (Martinez-Castellanos 2019).  $\gamma$ -rays above 100 TeV are attenuated by pair production on the extragalactic background light after propagating over a distance of tens of kiloparsecs.

panel of Figure 3). However, thanks to new surveys like the Australian Square Kilometre Array Pathfinder (ASKAP; Bannister et al. 2019) and the Canadian Hydrogen Intensity Mapping Experiment (CHIME)/FRB (CHIME/FRB Collaboration et al. 2018), the rate of FRB discoveries is rapidly growing and may reach thousands or more over the coming years.

The distribution of FRB energies  $dN/d\mathcal{E}_{\text{radio}} \propto \mathcal{E}_{\text{radio}}^{-\gamma}$  (where  $\gamma \lesssim 2$ ; Law et al. 2017; Lu & Piro 2019; Cruces et al. 2020; though see e.g., Gourdji et al. 2019) is such that the total radiated energy is dominated by the rarest, most energetic bursts. Given the neutrino radiative efficiency of the shocks  $\eta_\nu \propto \mathcal{E}_{\text{radio}}^{19/42}$  (Equation (35)), the total radiated neutrino energy is also dominated by the high- $\mathcal{E}_\nu$  bursts.

A key question then becomes the upper cut-off energy to the FRB energy distribution,  $\mathcal{E}_{r,\max}$ . Modeling the ASKAP FRB sample, Lu & Piro (2019) found a range of allowed values  $\mathcal{E}_{r,\max} \approx 3 \times 10^{42} - 2 \times 10^{44}$  erg for a burst frequency width  $\nu \sim 1.4$  GHz. In what follows, we optimistically assume<sup>9</sup>  $\mathcal{E}_{r,\max} \approx 10^{44}$  erg, bursts for which the local volumetric rate is estimated as  $\mathcal{R}(z=0) \sim 6$  Gpc $^{-3}$  yr $^{-1}$  (adopting a  $\gamma = 1.6$  power-law luminosity function; Lu & Piro 2019; Luo et al. 2020). At this rate, the closest FRB of this energy per year occurs at a distance  $D_{\min} \sim 0.34$  Gpc. Given its predicted neutrino energy  $\mathcal{E}_\nu \sim 5 \times 10^{43}$  erg (Equation (36)), its neutrino flux would be  $F_\nu \approx \mathcal{E}_\nu / (4\pi D_{\min}^2) \sim 10^{-9}$  GeV cm $^{-2}$ , i.e., still  $\sim 7$  orders of magnitude below the IceCube detection threshold.

The sensitivity could be improved by a stacked joint analysis of a large FRB sample (e.g., Aartsen et al. 2018; Kheirandish et al. 2019). Unfortunately, given the relatively long duration  $t_{\max} \sim 3000$  s for the most energetic  $\mathcal{E}_{\text{radio}} \approx 10^{44}$  erg bursts described above, the search becomes background-dominated after only a few bursts, after which the detector sensitivity quickly saturates. Although less-energetic FRBs are more common and produce shorter-lived neutrino bursts

<sup>9</sup> A burst of energy  $\mathcal{E}_{r,\max} \sim 10^{44}$  erg corresponds to a flare of energy  $\mathcal{E}_{\text{flare}} \sim 3 \times 10^{48}$  erg (Equation (9)), approaching the entire magnetic energy budget of a magnetar.

$t_{\max} \propto \mathcal{E}_{\text{radio}}^{4/7}$ , their sharply lower radiated energies  $\mathcal{E}_\nu \propto \mathcal{E}_{\text{radio}}^{61/42}$  largely cancel out these benefits.

In addition to a burst of neutrinos (from  $\pi^\pm$  decay), we predict a burst of  $\sim\text{TeV}$ – $\text{PeV}$  gamma-rays from neutral pion decay. As shown in Figure 4, the TeV thermal neutrinos fall in the sensitivity range of ground-based water Cherenkov detectors, including the Altitude Water Cherenkov Observatory (HAWC; Martinez-Castellanos 2019), and upcoming and future detectors such as the Large High Altitude Air Shower Observatory (LHAASO; di Sciascio & Lhaaso Collaboration 2016) and the Southern Wide-field Gamma-ray Observatory (SWG0; Huentemeyer et al. 2019). However, again for fiducial parameters we require a nearby source  $\lesssim 0.1$  kpc for a detection. Furthermore, the pion decay signal could be overwhelmed by nonthermal leptonic emission, depending on the electron acceleration efficiency of the shocks.

## 5. Conclusions

With the discovery of FRB 200428, flaring magnetars are the leading FRB model. However, several distinct mechanisms and environments around a magnetar for generating the radio burst—and any accompanying higher-frequency afterglow—have been proposed, which have proven challenging to distinguish observationally. A unique prediction of baryon-loaded shock-powered FRB models (Metzger et al. 2019; Margalit et al. 2020b) are neutrinos generated by ions heated or accelerated at the shock interact with thermal synchrotron shock photons via the photohadronic process.

We predict a burst of  $\sim\text{TeV}$ – $\text{PeV}$  neutrinos of total energy  $\mathcal{E}_\nu \sim 10^{35}$ – $10^{44}$  erg (depending most sensitively on the FRB isotropic energy; Equation (36)) which lasts for a timescale  $t_{\max} \sim 0.1$ – $1000$  s (Equation (25)) following the radio burst (once accounting for the time delay due to the finite propagation speed of the radio waves as inferred from the dispersion measure). Our calculations make several optimistic assumptions, including (1) nonthermal particle acceleration at magnetized shocks with an efficiency of 10%; (2) the presence of a baryon-loaded medium which extends at least a distance  $r_{\max} \equiv r[t_{\max}] \sim (3\text{--}30)r_{\text{FRB}}$  beyond the radius  $r_{\text{FRB}}$  probed by the FRB emission itself.<sup>10</sup>

Although the detection prospects with present neutrino observatories are extremely challenging (to put it lightly), the detection of even a single neutrino from an FRB would be a smoking gun for this model. The most promising potentiality is a giant flare from a nearby Galactic magnetar with the fortuitous geometry of the shock-generating plasmoid being directed along our line of sight.

We thank Ali Kheirandish for helpful discussion about IceCube sensitivities to FRBs. We thank Israel Martinez for helpful discussion about HAWC sensitivities to bursts. B.D.M. acknowledges support from the Simons Foundation (grant 606260). Support for K.F. was provided by NASA through the NASA Hubble Fellowship grant #HST-HF2-51407 awarded by the Space Telescope Science Institute, which is operated by the Association of Universities for Research in Astronomy,

<sup>10</sup> We have additionally assumed, for simplicity, a constant density profile for this upstream medium; however, our results are not particularly sensitive to this choice. As an example, for fiducial FRB parameters and  $k = -2$  instead of  $k = 0$  (where  $n_{\text{ext}} \propto r^{-k}$ ) we find that the peak neutrino efficiency  $\eta_\nu[t_{\max}]$  is only increased by a modest factor of  $\sim 5$ . Similarly, a positive  $k = 2$  would decrease the efficiency by a factor of  $\sim 4$ .

Inc., for NASA, under contract NAS5-26555. B.M. is supported by NASA through the NASA Hubble Fellowship grant #HST-HF2-51412.001-A awarded by the Space Telescope Science Institute, which is operated by the Association of Universities for Research in Astronomy, Inc., for NASA, under contract NAS5-26555.

## ORCID iDs

Brian D. Metzger  <https://orcid.org/0000-0002-4670-7509>

## References

- Aartsen, M. G., Ackermann, M., Adams, J., et al. 2018, *ApJ*, 857, 117  
Aartsen, M. G., Ackermann, M., Adams, J., et al. 2020, *ApJ*, 890, 111  
Babul, A.-N., & Sironi, L. 2020, *MNRAS*, in press  
Bannister, K. W., Deller, A. T., Phillips, C., et al. 2019, *Sci*, 365, 565  
Beloborodov, A. M. 2017, *ApJL*, 843, L26  
Beniamini, P., & Kumar, P. 2020, *MNRAS*, 498, 651  
Berezinskii, V. S., Bulanov, S. V., Dogiel, V. A., & Ptuskin, V. S. 1990, in *Astrophysics of Cosmic Rays*, ed. V. L. Ginzburg (Amsterdam: North-Holland)  
Blandford, R. D., & McKee, C. F. 1976, *PhFl*, 19, 1130  
Blandford, R. D., & Ostriker, J. P. 1978, *ApJL*, 221, L29  
Bochenek, C. D., McKenna, D. L., Belov, K. V., et al. 2020, *PASP*, 132, 034202  
CHIME/FRB Collaboration, Amiri, M., Bandura, K., et al. 2018, *ApJ*, 863, 48  
CHIME/FRB Collaboration, Andersen, B. C., Bandura, K., et al. 2019, *ApJL*, 885, L24  
Cordes, J. M., & Chatterjee, S. 2019, *ARA&A*, 57, 417  
Cruces, M., Spitler, L. G., Scholz, P., et al. 2020, arXiv:2008.03461  
Dermer, C. D., & Atoyan, A. 2003, *PhRvL*, 91, 071102  
di Sciascio, G. & Lhaaso Collaboration 2016, *NPPP*, 279–281, 166  
Frail, D. A., Kulkarni, S. R., & Bloom, J. S. 1999, *Natur*, 398, 127  
Gaensler, B. M., McClure-Griffiths, N. M., Oey, M. S., et al. 2005, *ApJL*, 620, L95  
Gallant, Y. A., Hoshino, M., Langdon, A. B., Arons, J., & Max, C. E. 1992, *ApJ*, 391, 73  
Gelfand, J. D., Lyubarsky, Y. E., Eichler, D., et al. 2005, *ApJL*, 634, L89  
Giannios, D., & Spitkovsky, A. 2009, *MNRAS*, 400, 330  
Gourdji, K., Michilli, D., Spitler, L. G., et al. 2019, *ApJL*, 877, L19  
Guetta, D., & Granot, J. 2003, *PhRvL*, 90, 201103  
Hessels, J. W. T., Spitler, L. G., Seymour, A. D., et al. 2019, *ApJL*, 876, L23  
Huentemeyer, P., BenZvi, S., Dingus, B., et al. 2019, *BAAS*, 51, 109  
Iwamoto, M., Amano, T., Hoshino, M., et al. 2019, *ApJL*, 883, L35  
Katz, J. I. 2016, *ApJ*, 826, 226  
Kelner, S. R., & Aharonian, F. A. 2008, *PhRvD*, 78, 034013  
Kheirandish, A., Pizzuto, A., & Vandenbroucke, J. 2019, arXiv:1909.00078  
Kulkarni, S. R., Ofek, E. O., Neill, J. D., Zheng, Z., & Juric, M. 2014, *ApJ*, 797, 70  
Kumar, P., Lu, W., & Bhattacharya, M. 2017, *MNRAS*, 468, 2726  
Law, C. J., Abuzzo, M. W., Bassa, C. G., et al. 2017, *ApJ*, 850, 76  
Lorimer, D. R., Bailes, M., McLaughlin, M. A., Narkevic, D. J., & Crawford, F. 2007, *Sci*, 318, 777  
Lu, W., Kumar, P., & Zhang, B. 2020a, *MNRAS*, 498, 1397  
Lu, W., & Piro, A. L. 2019, *ApJ*, 883, 40  
Lu, W., Piro, A. L., & Waxman, E. 2020b, *MNRAS*, 498, 1973  
Luo, R., Men, Y., Lee, K., et al. 2020, *MNRAS*, 494, 665  
Lyubarsky, Y. 2014, *MNRAS*, 442, L9  
Margalit, B., Beniamini, P., Sridhar, N., & Metzger, B. D. 2020a, *ApJL*, 899, L27  
Margalit, B., Metzger, B. D., & Sironi, L. 2020b, *ApJL*, 899, L27  
Martinez-Castellanos, I. 2019, arXiv:1908.06122  
Mereghetti, S., Savchenko, V., Ferrigno, C., et al. 2020, arXiv:2005.06335  
Mészáros, P., & Waxman, E. 2001, *PhRvL*, 87, 171102  
Metzger, B. D., Berger, E., & Margalit, B. 2017, *ApJ*, 841, 14  
Metzger, B. D., Margalit, B., & Sironi, L. 2019, *MNRAS*, 485, 4091  
Murase, K., Kashiyama, K., & Mészáros, P. 2016, *MNRAS*, 461, 1498  
Particle Data Group, Eidelman, S., Hayes, K. G., et al. 2004, *PhLB*, 592, 1  
Petroff, E., Burke-Spolaor, S., Keane, E. F., et al. 2017, *MNRAS*, 469, 4465  
Petroff, E., Hessels, J. W. T., & Lorimer, D. R. 2019, *A&ARv*, 27, 4  
Platts, E., Weltman, A., Walters, A., et al. 2019, *PhR*, 821, 1  
Plotnikov, I., & Sironi, L. 2019, *MNRAS*, 485, 3816  
Popov, S. B., & Postnov, K. A. 2013, arXiv:1307.4924



- Ravi, V., Shannon, R. M., Bailes, M., et al. 2016, *Sci*, 354, 1249
- Ridnaia, A., Svinkin, D., Frederiks, D., et al. 2020, arXiv:2005.11178
- Sironi, L., & Spitkovsky, A. 2011, *ApJ*, 726, 75
- Spitler, L. G., Scholz, P., Hessels, J. W. T., et al. 2016, *Natur*, 531, 202
- Tavani, M., Casentini, C., Ursi, A., et al. 2020, arXiv:2005.12164.
- Tendulkar, S. P., Kaspi, V. M., & Patel, C. 2016, *ApJ*, 827, 59
- The CHIME/FRB Collaboration, Andersen, B. C., Bandura, K. M., et al. 2020, arXiv:2005.10324
- The IceCube-Gen2 Collaboration, Aartsen, M. G., Abbasi, R., et al. 2020, arXiv:2008.04323
- Thornton, D., Stappers, B., Bailes, M., et al. 2013, *Sci*, 341, 53
- Vandenbroucke, J. 2020, *ATel*, 13689, 1
- Waxman, E., & Bahcall, J. 1997, *PhRvL*, 78, 2292
- Waxman, E., & Bahcall, J. 1999, *PhRvD*, 59, 023002
- Yamasaki, S., Kashiyama, K., & Murase, K. 2020, arXiv:2008.03634
- Yuan, Y., Beloborodov, A. M., Chen, A. Y., & Levin, Y. 2020, *ApJL*, 900, L21
- Zhang, S.-N., Xiong, S. L., Li, C. K., et al. 2020, *GCN*, 27675, 1